Front. Struct. Civ. Eng. 2020, 14(6): 1299–1315
https://doi.org/10.1007/s11709-020-0712-6

TRANSDISCIPLINARY INSIGHT

An artificial neural network model on tensile behavior of hybrid steel-PVA fiber reinforced concrete containing fly ash and slag power

Fangyu LIU[a], Wenqi DING[b,c*], Yafei QIAO[b,c*], Linbing WANG[a]

[a] *Department of Civil and Environmental Engineering, Virginia Polytechnic Institute and State University, Blacksburg, VA 24061, USA*

[b] *Department of Geotechnical Engineering, College of Civil Engineering, Tongji University, Shanghai 200092, China*

[c] *Key Laboratory of Geotechnical and Underground Engineering (Tongji University), Ministry of Education, Shanghai 200092, China*

[*] *Corresponding author. E-mails: yafei.qiao@tongji.edu.cn; dingwq@tongji.edu.cn*

ABSTRACT The tensile behavior of hybrid fiber reinforced concrete (HFRC) is important to the design of HFRC and HFRC structure. This study used an artificial neural network (ANN) model to describe the tensile behavior of HFRC. This ANN model can describe well the tensile stress-strain curve of HFRC with the consideration of 23 features of HFRC. In the model, three methods to process output features (no-processed, mid-processed, and processed) are discussed and the mid-processed method is recommended to achieve a better reproduction of the experimental data. This means the strain should be normalized while the stress doesn't need normalization. To prepare the database of the model, both many direct tensile test results and the relevant literature data are collected. Moreover, a traditional equation-based model is also established and compared with the ANN model. The results show that the ANN model has a better prediction than the equation-based model in terms of the tensile stress-strain curve, tensile strength, and strain corresponding to tensile strength of HFRC. Finally, the sensitivity analysis of the ANN model is also performed to analyze the contribution of each input feature to the tensile strength and strain corresponding to tensile strength. The mechanical properties of plain concrete make the main contribution to the tensile strength and strain corresponding to tensile strength, while steel fibers tend to make more contributions to these two items than PVA fibers.

KEYWORDS artificial neural network, hybrid fiber reinforced concrete, tensile behavior, sensitivity analysis, stress-strain curve

1 Introduction

Fiber reinforced concrete (FRC) has become a prevalent type of concrete and widely used in many civil infrastructures [1–3], because of its improvement in mechanical properties [4–6] and durability [7,8]. Many types of fibers, including steel fibers, polyvinyl alcohol (PVA) fibers, polypropylene (PP) fibers, and basalt fibers, have been used to produce FRC [3,7,9,10]. For a given fiber type, the geometry and the volume content of fibers could significantly influence the mechanical properties of concrete [11–15]. Moreover, the hybridization of different fibers could enhance reinforcement [13]. Therefore, hybrid fiber reinforced concrete (HFRC) was developed [16] and two different types of fibers are usually adopted. For example, steel fiber, a type of macrofibers, and PVA fiber, a type of microfibers, are often used to prepare the HFRC, which has more improvement in the mechanical behavior than the steel or PVA FRC alone.

Constitutive modeling of HFRC is important for the design of the HFRC structure. Many constitutive models of HFRC has been proposed to present the stress-strain relationship of HFRC [10,17,18] by considering many fiber characteristics. But it is hard to develop one model

Article history: Received Aug 4, 2020; Accepted Oct 26, 2020

from a purely mathematical perspective because of the complexity of HFRC, such as the strain-softening/hardening, and volumetric dilatancy [17]. Recently, the deep learning method has been successfully applied in modeling concrete to overcome these limitations [19,20]. As one of the basic deep learning methods, artificial neural network (ANN) has become a popular method to model the mechanical properties of FRC [20], to design the mix compositions of FRC [19], to describe the stress-strain model of FRC [21], to predict the fracture energy of polymer-nanoparticle composites (PNCs) [22,23], to compute the flexoelectricity effect in truncated pyramid structures [24], to build a deep collocation method for thin plate bending problems [25], to solve boundary values problem [26], and to act as function approximation machines to approximate the solution of partial differential equations [27]. Compared with the conventional constitutive model, the ANN model could consider more factors and provide a better prediction of the mechanical properties of concrete. However, few ANN models were proposed to predict the whole stress-strain curve of HFRC and to investigate the effect of HFRC's contents on its mechanical behavior.

Although the ANN model could implicitly detect complex nonlinear relationships between dependent and independent variables, it is usually recognized as 'black boxes' that provide little information about relationships among different variables, and therefore, are difficult to be understood [28]. Sensitivity analysis has been proposed to explain how the uncertainty in the output of the ANN model can be divided and allocated to different sources of uncertainty in its inputs [29,30]. There are several methods to investigate the sensitivity of the ANN model: the 'PaD' method (Partial Derivatives), the 'Weights' method, the 'Profile' method, and the 'Stepwise' method [30]. Considering the values of the inputs and weights, the 'PaD' method could overcome some disadvantages of other methods and be an easy method to calculate the contribution of each input feature [28].

Therefore, this study aims to develop a new approach to describe the tensile stress-strain curve of HFRC by using the ANN model; and to highlight the ability of the ANN model by investigating the effect of different contents of HFRC on the tensile behavior of HFRC. To make a better prediction and consider experimental conditions, many factors are introduced into the ANN model, including the fiber characteristics (fiber volume, weight, length, diameter, the aspect ratio, and the reinforcement index), mechanical properties of plain concrete (elastic modulus, compressive strength, and strain corresponding to tensile strength (SCTS)), and the composition of concrete mixture (cement, fly ash, slag powder, water, coarse aggregate, fine aggregate, and water binder ratio). Moreover, three methods used to process output features are also assessed and compared.

In the following sections, the framework of the ANN model is first introduced. Then experimental results of many direct tensile tests on HFRC carried out by our group [9] and other data from previous literature are used to build the database. After that, the ANN model is trained and evaluated based on the database, meanwhile the equation-based model is also built. The comparison between these two models is made via the description of the experiment data. The results of three processed methods are discussed and the most suitable method for the ANN model is recommended. The sensitivity analysis is finally done to show how input features make contributions to output features of the ANN model.

2 Framework of the ANN model

2.1 ANN Approach

Typically, ANN has three main layers: the input layer, hidden layer, and output layer. The architecture of the ANN model plays an essential role in building such a model. Different hidden neurons and different hidden layers are investigated, and 5-fold cross-validation [31] is used to evaluate and get a better ANN model. Figure 1 shows the procedure 5-fold cross-validation which includes finding better parameters, such as neurons and hidden layers, on the training dataset and making the final evaluation on the test dataset. During the first procedure, the training dataset is split into the inner training dataset (blue block in Fig. 1) and the validation dataset (green block in Fig. 1). The maximal epoch is 80 during the cross-validation. The cross-validation results reveal that 2-hidden-layer are most suitable for the ANN model in this work. Figure 2 shows the architecture of the used ANN model, including one input layer, 2-hidden-layer, and one output layer.

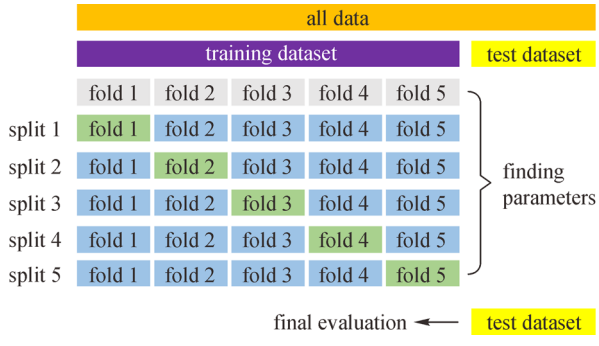

Fig. 1 5-fold cross-validation.

The calculation process of the ANN approach is that considering the input vector of one neuron in one layer is $\boldsymbol{x} = [x_1, x_2, ..., x_m]$, the neuron in the next layer is computed: 1) $\boldsymbol{x}$ will be multiplied by the weight; 2) the value of the neuron in the next layer z is obtained by the activation function, as shown in Eq. (1).

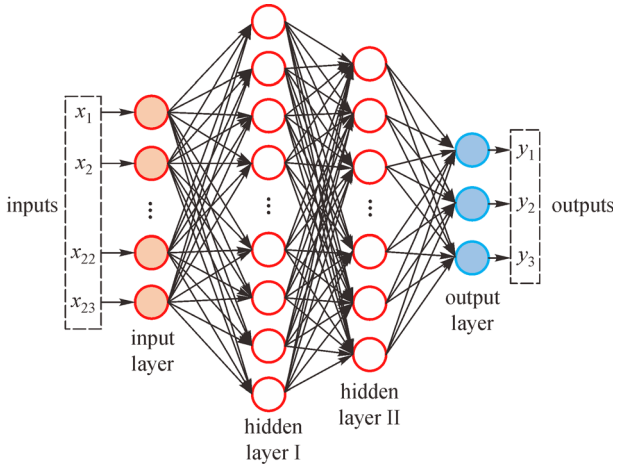

Fig. 2 Scheme of the ANN approach in this study.

$$z = f(\omega^{\mathrm{T}}\boldsymbol{x} + b) = f\left(\sum_{i=1}^{m}\omega_i x_i + b\right),\ x \in R^{1\times m},$$

$$\omega \in R^{1\times m},\ z \in R. \tag{1}$$

As increasing the nonlinearity of the neural network, the activation function plays an important role in the neural network. This study uses the popular activation function, the rectified linear unit (ReLU) function [32], which is

$$f(x) = \max(0,x). \tag{2}$$

2.2 Procedures of the ANN model

There are four main procedures of the ANN model to describe the tensile behavior of HFRC, as illustrated in Fig. 3, including the dataset preprocess, dataset splitting, the ANN model training and evaluating, and prediction.

2.2.1 Dataset preprocess

The quality of the dataset has a strong influence on the performance of the ANN model. Therefore, several tensile test results of HFRC which this research group did before are combined with the relevant data collected in Refs. [9,10,33–35] to improve the quantity and diversity of the dataset. Since the ANN model is used to predict the tensile stress-strain curve, the dataset would include many tensile stress-strain curves of HFRC rather than only the tensile strength and SCTS. According to the factors influencing the tensile behavior of HFRC, the input data has a total of 23 features in this study, which are summarized in Table 1. Correspondingly, the output data are the stress, the tensile strength of HFRC, and the SCTS of HFRC, which could be used to obtain the tensile stress-strain curve and evaluate the tensile behavior of HFRC.

The raw dataset needs preprocessing because the amplitude and the range of different input features vary a lot and could have a significant influence on the prediction of the ANN model. For example, the strain of HFRC varies from 0 to 0.01 and it has at least 1000 data points for one HFRC specimen, but the weight of the cement only has two options (225 and 449 kg/m^3) which are far higher than the maximal strain. Without normalization, large differences among input features could make it hard to train and evaluate the ANN model. Therefore, before training and evaluating the ANN model, the input data needs normalization and the Min-Max Scaling method is used in this work. The Min-Max Scaling could normalize the data to a range from 0 to 1 by using the following equation,

$$x_{j,\mathrm{scaled}}^{(i)} = \frac{x_j^{(i)} - x_{\min}^{(i)}}{x_{\max}^{(i)} - x_{\min}^{(i)}}, \tag{3}$$

where i = 1,2,…,m (m is the number of features), j = 1,2,…,n (n is the number of data samples); $x_{\max}^{(i)}$ and

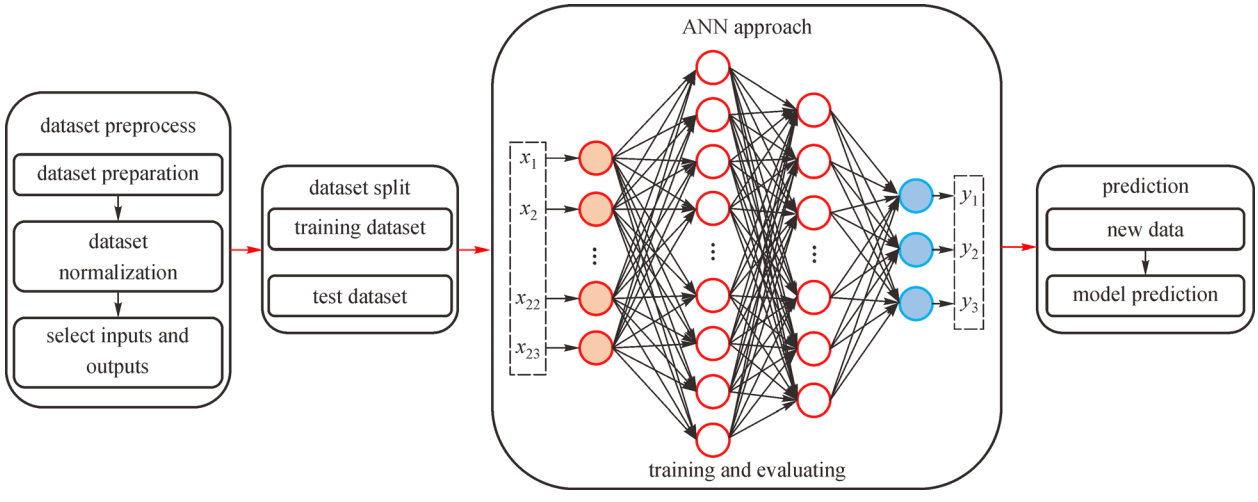

Fig. 3 Framework of the ANN model in this study.

Table 1 Features of the input data

parts	feature
strain	strain
steel fiber	fiber volume of steel fiber
	weight of steel fiber
	length of steel fiber
	diameter of steel fiber
	aspect ratio of steel fiber
	reinforcement index of steel fiber
PVA fiber	fiber volume of PVA fiber
	weight of PVA fiber
	length of PVA fiber
	diameter of PVA fiber
	aspect ratio of PVA fiber
	reinforcement index of PVA fiber
mechanical properties of plain concrete	elastic modulus of plain concrete
	tensile strength of plain concrete
	strain corresponding to tensile strength of plain concrete
components of HFRC	weight of the cement
	weight of fly ash
	weight of slag powder
	weight of water
	weight of coarse aggregate
	weight of fine aggregate
	water binder ratio

$x_{\min}^{(i)}$ are the maximal and minimal values of the ith feature, respectively; $x_j^{(i)}$ is the original jth data sample of the ith feature, and $x_{j,\text{scaled}}^{(i)}$ is the scaled jth data sample of the ith feature. The Min-Max Scaling is completed by the preprocessing module of scikit-learn [36].

There is also a large difference among different output features, like the tensile strength of HFRC (greater than 3 MPa) and the SCTS of HFRC (less than 0.03), so it would be better to normalize output features. To illustrate this normalization effect, this study uses three methods to process output features: no-processed, mid-processed, and processed. No-processed means that output features keep their original value and mid-processed means that only the SCTS of HFRC is normalized. Processed means that all three output features are normalized. Because of applying three methods to process output features, triplicate ANN models use these three methods separately and are trained and evaluated in parallel.

2.2.2 Dataset split

The dataset needs to be separated into two subsets, the training dataset and the test dataset, to train and evaluate the ANN model. After shuffling the whole dataset, it is randomly split into the training and test dataset via the model selection module of scikit-learn, 'train_test_split' [36]. The training dataset, 70% of the whole dataset, is used to train the ANN model; and the test dataset, the other 30% of the whole dataset, is used to evaluate the ANN model.

2.2.3 ANN model training and evaluating

The ANN model (Fig. 2) runs on the popular deep learning library of Pytorch [37] and Skorch [38]. As this is the regression problem, the loss function adopts the mean square error (*MSE*) function. The used optimizer is the adaptive moment estimation (Adam) [39] and the batch size of the dataset is 128. The maximal epoch is 1000 epochs; during each epoch, the ANN model is first trained by the training dataset and then evaluated by the test dataset. Meanwhile, the losses of the training dataset and test dataset are printed and compared to ensure that neither underfitting nor overfitting happens.

The learning rate is a crucial hyperparameter which determines how fast the parameters are updated. The initial learning rate is 0.01; when the decreasing rate of loss value is limited (i.e., 480 epochs in this work), the learning rate would be reduced by 0.1 times. The learning rate decay could improve the convergence of the ANN model.

After finishing training the ANN model, the parameters of the ANN model would be saved to predict the new data and do the sensitivity analysis.

2.2.4 Prediction

The new input dataset is fed into the ANN model after completing training the ANN model. As mentioned above, each data has three output features: stress, tensile strength, and SCTS. The predicted stress is combined with the input strain to obtain the tensile stress-strain curve. The final predicted tensile strength and SCTS of each HFRC sample are determined by the mean value of these two items of each HFRC sample's data.

3 Database of the tensile behavior of HFRC

To build the database, experimental data of a series of direct tensile tests on HFRC containing fly ash and slag powder performed by our group [9], as well as the relevant data in the literature, were used. Table 2 summarizes the key information of all collected data. As different cementitious materials seem to have no significant influence on the tensile behavior of HFRC [9], all these data are combined to prepare the database.

To describe the tensile stress-strain curves, the whole

Table 2 The steel-PVA fiber hybridization of HFRC from previous literature

cementitious material	fiber volume (%)		fiber length (mm)		fiber diameter (mm)		Ref.
	steel fiber	PVA fiber	steel fiber	PVA fiber	steel fiber	PVA fiber	
cement + fly ash + slag powder (HFRC)	0.5	0.5	38	12	0.677	0.039	[9]
	0.5	1.0					
	0.5	1.5					
	1.0	0.5					
	1.0	1.0					
	1.0	1.5					
	1.5	0.5					
	1.5	1.0					
	1.5	1.5					
cement (HFRC)	0.8	0.1	35/50	8/12	0.55/0.75	0.04	[10]
	0.8	0.2					
	1.3	0.1					
	1.3	0.2					
cement (HFRC)	0.05	0.15	38	12	1.10	0.04	[33]
	0.1	0.3					
	0.3	0.6					
	0.03	0.17					
	0.06	0.34					
	0.11	0.69					
	0.02	0.18					
	0.04	0.36					
	0.08	0.72					
cement (HFRC)	0.25	0.07	12/15	30/60	0.5/0.73	0.015	[34]
	0.25	0.14					
	0.51	0.07					
	0.51	0.14					
cement + GGBS* + silica fume (HFRC)	0.25	0.25	20	6	0.4	0.12	[35]
	0.5	0.25					
	0.75	0.25					
	1	0.25					
	1.25	0.25					
	0.25	0.25					

*Note: GGBS: Ground-granulated blast-furnace slag.

dataset of these curves is necessary. This is the main difference of the dataset comparing to other ANN models that only focus on the tensile strength or the SCTS. The direct tensile test can be used to obtain these stress-strain curves, while the dog bone-shaped specimen is suggested to be used [9]. Figure 4 shows the typical experimental tensile stress-strain curves of HFRC. The black line is the average tensile stress-strain curve of each type of HFRC and the gray area is drawn by all tensile stress-strain curves of each type of HFRC. The tensile strength and SCTS are also illustrated in Fig. 4. Model details about the tests and results can be found in Ref. [9].

With all these data, the main characters of each feature in the output and input can be identified. Table 3 summarizes the mean value, the medium value, and the standard deviation of each feature in the database. The size of the whole dataset is 9081. Among all output features, the tensile strength has the biggest mean value and median value, while the tensile stress has the biggest standard deviation. All these values of the SCTS are relatively

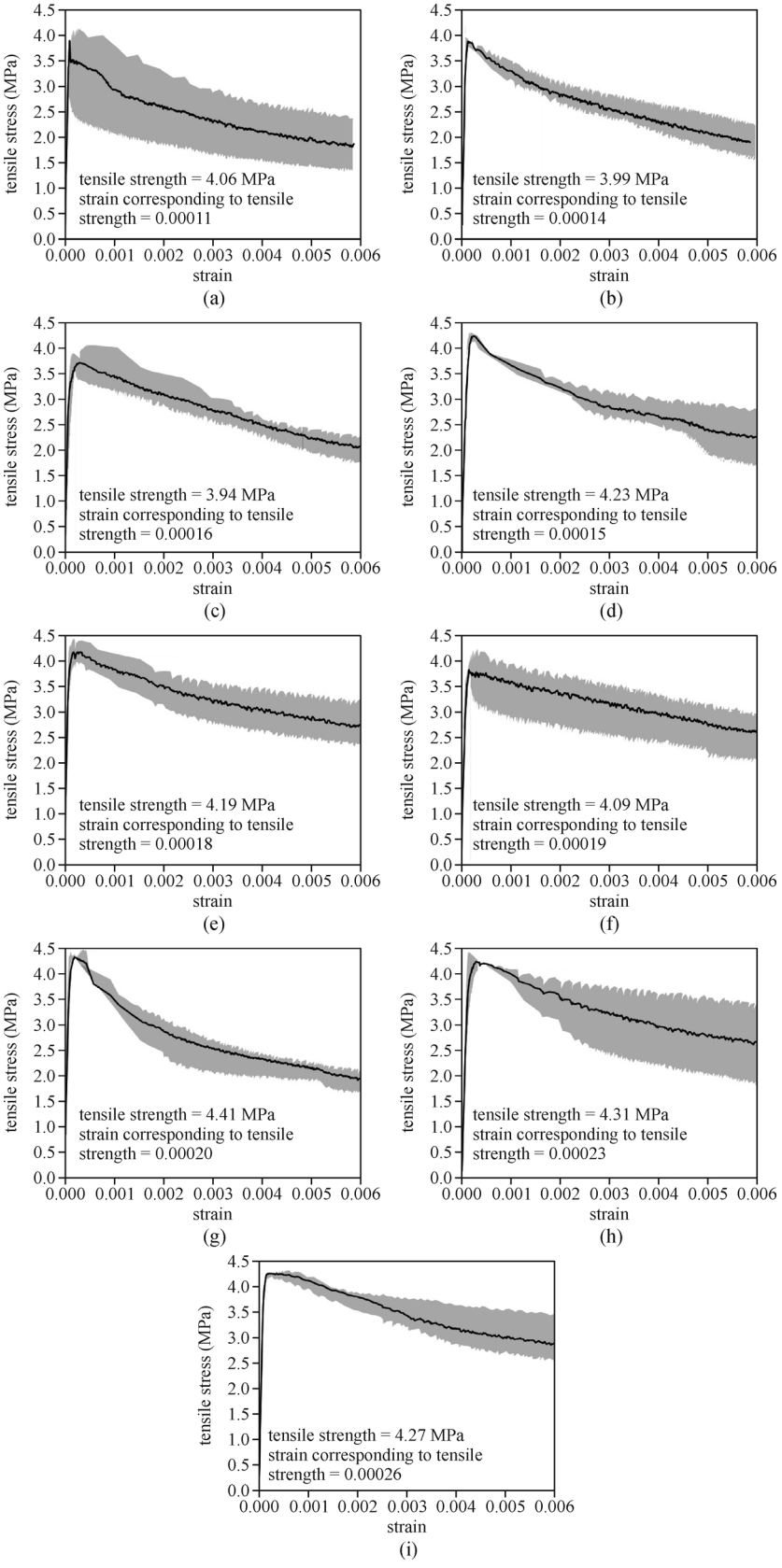

Fig. 4 Tensile stress-strain curves of (a) $S_{0.5}P_{0.5}$, (b) $S_{0.5}P_{1.0}$, (c) $S_{0.5}P_{1.5}$, (d) $S_{1.0}P_{0.5}$, (e) $S_{1.0}P_{1.0}$, (f) $S_{1.0}P_{1.5}$, (g) $S_{1.5}P_{0.5}$, (h) $S_{1.5}P_{1.0}$, (i) $S_{1.5}P_{1.5}$.

Table 3 Summary of the dataset for the ANN model (size = 9801)

type	feature	mean	median	standard deviation
output	tensile stress	2.40	2.47	0.97
	tensile strength	4.10	4.02	0.20
	strain corresponding to tensile strength	0.000253	0.000168	0.000172
input	strain	0.002542	0.001309	0.003017
	fiber volume of steel fiber	1.04	1.00	0.38
	weight of steel fiber	81.84	78.50	29.79
	length of steel fiber	39.53	38.00	4.54
	diameter of steel fiber	0.68	0.68	0.05
	aspect ratio of steel fiber	58.51	56.13	4.13
	reinforcement index of steel fiber	0.61	0.56	0.22
	fiber volume of PVA fiber	0.81	1.00	0.52
	weight of PVA fiber	10.56	13.00	6.81
	length of PVA fiber	11.59	12.00	1.21
	diameter of PVA fiber	0.04	0.04	0.00
	aspect ratio of PVA fiber	295.53	307.69	32.32
	reinforcement index of PVA fiber	2.48	3.08	1.64
	elastic modulus of plain concrete	35915	35369	1135
	tensile strength of plain concrete	3.28	3.41	0.21
	strain corresponding to tensile strength of plain concrete	0.000087	0.000088	0.000019
	weight of the cement	282	225	98
	weight of fly ash	56	75	33
	weight of slag powder	56	75	33
	weight of water	174	165	16
	weight of coarse aggregate	1019	1024	8
	weight of fine aggregate	756	785	50
	water binder ratio	0.443	0.440	0.004

small, which may affect the training process and will be discussed in section 4.2.

4 Performance of the ANN model

4.1 Indices for evaluating model

Several indices have been introduced to combine with the loss to evaluate the performance of the ANN model, including the coefficient of determination (R^2) and mean absolute error (*MAE*) [21]. R^2 is defined in Eq. (4); the closer its value is to 1, the better the prediction of the ANN model fits with the true data. *MAE* is determined in Eq. (5) and it is similar to the loss to evaluate the ANN model; the smaller the *MAE* is, the better the performance of the ANN model is:

$$R^2(y,\hat{y}) = 1 - \frac{\sum_{k=1}^{n}(y_k - \hat{y_k})^2}{\sum_{k=1}^{n}(y_k - \overline{y})^2}, \quad \overline{y} = \frac{1}{n}\sum_{k=1}^{n} y_k, \tag{4}$$

$$MAE(y,\hat{y}) = \frac{1}{n}\sum_{k=1}^{n}|y_k - \hat{y_k}|, \tag{5}$$

where $\hat{y}$ is the predicted value, y is the true value, $\hat{y_k}$ is the predicted value of the kth sample, and y_k is the true value of the kth sample.

4.2 ANN model training and evaluating

The ANN model is trained and evaluated using the database presented in Section 3. As the 5-fold cross-validation is employed to find the better ANN model, Figs. 5(a) and 5(b) show the R^2 of the training dataset and validation dataset for the 2-hidden-layer and 3-hidden-layer ANN models, while the Sigmoid function is also acted as the activation function to make a comparison. Meanwhile, some typical machine learning methods, such as support vector machine (SVM) [40], random forests (an ensemble learning method) [41], Gaussian Processes [42], are also used to make a comparison with the ANN model. Figure 5(c) shows the R^2 of the test dataset for these seven

models. Although the 3-hidden-layer ANN model with ReLU has the highest R^2 of the validation dataset, its R^2 of the test dataset is a little lower than that of the 2-hidden-layer ANN model with ReLU. Both the 2-hidden-layer and 3-hidden-layer ANN models with ReLU are higher than that with Sigmoid in terms of the R^2 of the validation dataset and test dataset, as shown in Fig. 5. Therefore, ReLU is adopted as the activation function in the following analysis. Compared with the ANN model, these three typical machine learning methods have a lower R^2 of the test dataset.

According to Fig. 5, the ANN model with 80 neurons in the hidden layer I and 10 neurons in the hidden layer II is used. Then, training and evaluating this ANN model is followed by the procedure in Section 2.2. Figure 6 shows the loss curves, R^2 curves, and *MAE* curves of the training dataset and test dataset. The loss values of the training dataset and test dataset (Fig. 6(a)) drop nonlinearly and rapidly before 480 epochs and then they tend to remain stable and converge. This is because the learning rate changes from 0.01 to 0.001 at the 480 epochs. The lowest flat part could be found in all loss curves after 960 epochs because the learning rate changes from 0.001 to 0.0001. The learning rate determines how fast the model

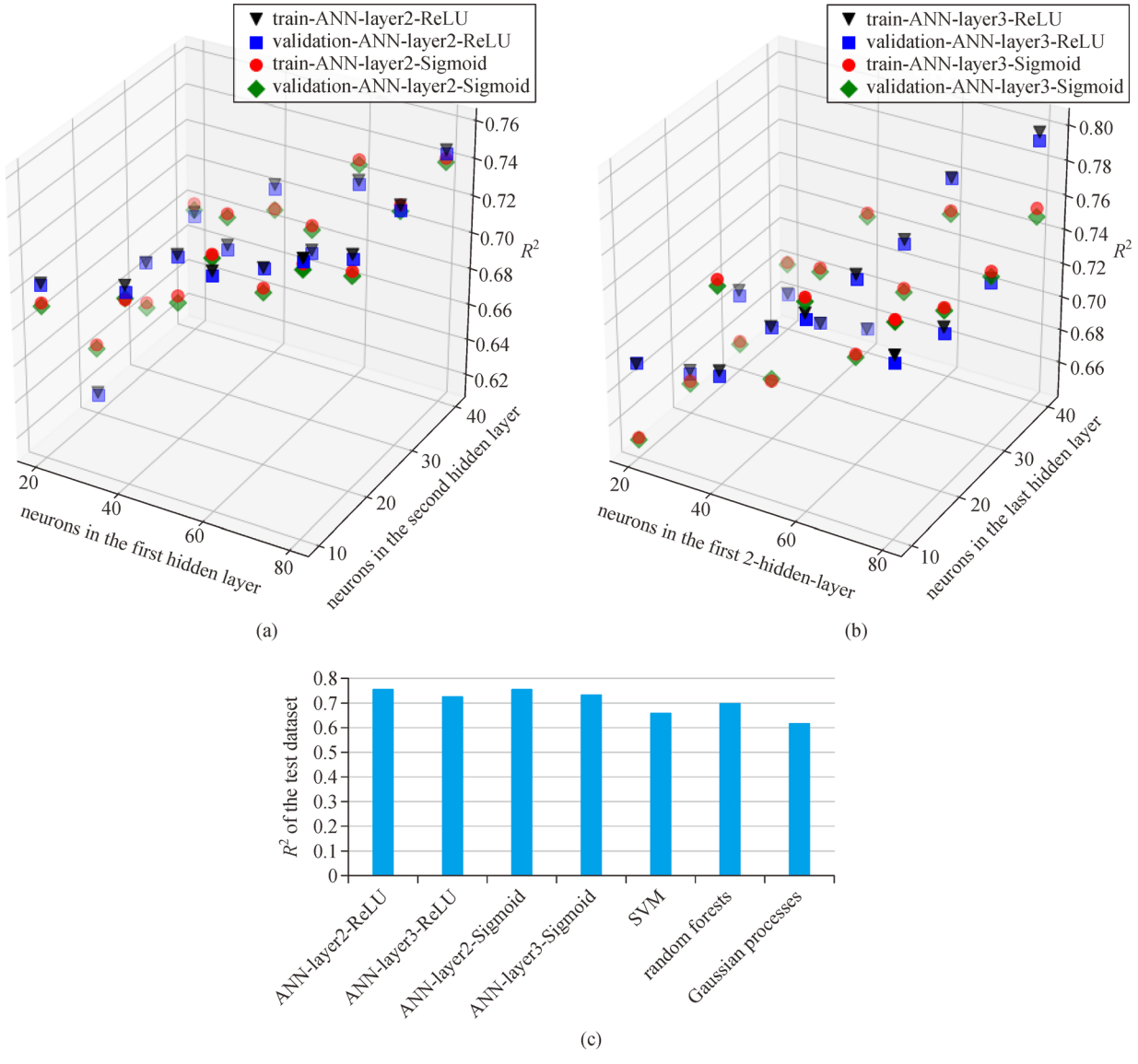

Fig. 5 R^2 of the training and validation dataset for: (a) the 2-hidden-layer ANN model with ReLU and Sigmoid, respectively; (b) the 3-hidden-layer ANN model with ReLU and Sigmoid, respectively; (c) R^2 of the test dataset for the 2-hidden-layer ANN model with ReLU and Sigmoid, respectively, the 3-hidden-layer ANN model with ReLU and Sigmoid respectively, SVM, Random Forests, Gaussian Processes.

converges. The big learning rate could make the loss decrease quickly but not smoothly, which is usually used in early training. As the learning rate becomes smaller, the loss tends to vary slowly, which could help the model more easily converge in the late period.

Three obvious patterns of loss curves could be found in Fig. 6(a). This is induced by the three different processed methods of output features presented in Section 2. The loss

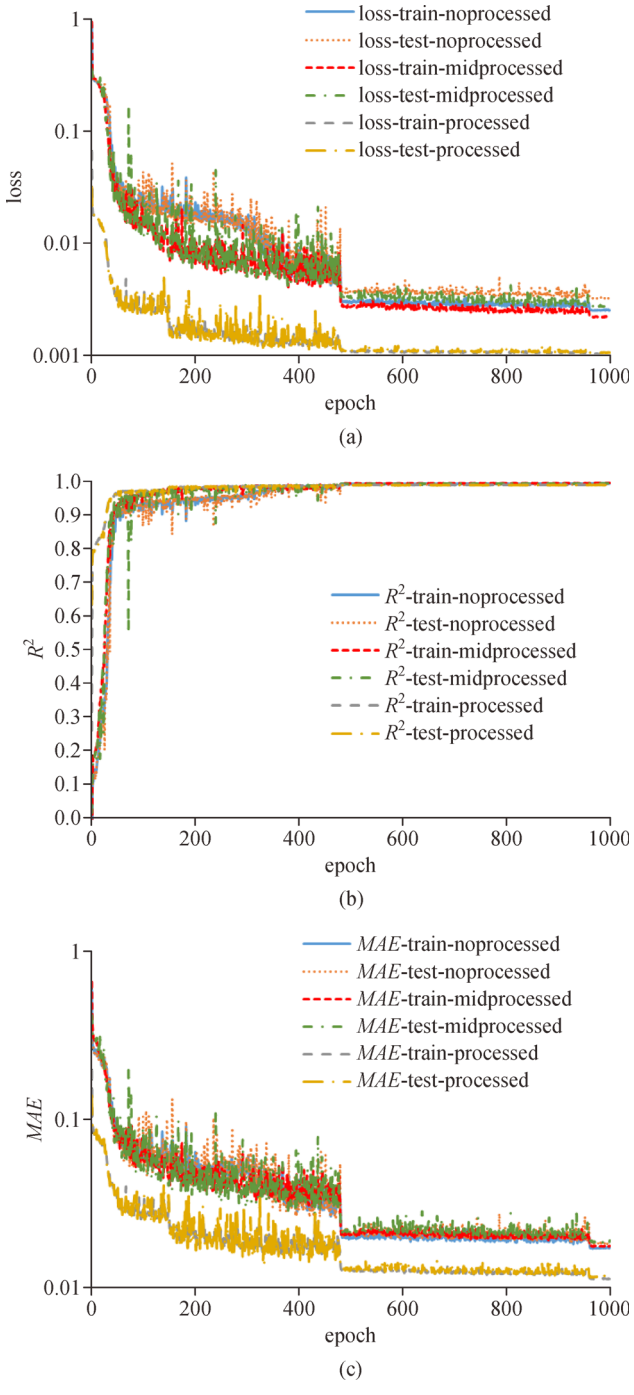

Fig. 6 Training and evaluating results of the ANN model: (a) loss; (b) R^2; (c) *MAE*.

of the no-processed method is the highest among the three processed methods no matter the loss belongs to the training dataset or the test dataset. As the degree of processing improves, the loss of the training dataset and test dataset decrease. This is because the Min-Max Scaling could limit the data in a small area (like 0 to 1) and enable the data to distribute evenly. For example, 3.113 and 4.022 MPa are the test data and the difference between these two values is 0.909 MPa. After the Min-Max Scaling, the corresponding data are 0.697 and 0.907, and the difference decreases to 0.21. The decrease of the range and the difference could enable the gap between the prediction and test data to become smaller, leading to a decrease of the loss (Fig. 6(a)).

The R^2 and *MAE* of the training dataset and test dataset are shown in Figs. 6(b) and 6(c). There are two patterns of *MAE* curves for three processed methods; the normalized output features have the lowest *MAE* of the training dataset and test dataset. In contrast, there is no obvious difference between the R^2 of these three processed methods. All R^2 of the training dataset and test dataset increase dramatically to 0.9 before 49 epochs, then gradually rise and finally reach a value higher than 0.99. All these indices reveal the good reliability of the ANN model.

4.3 Equation-based model

An equation-based model is also proposed based on the constitutive model recommended in GB 50010-2010 [43] to compare with the ANN model. The tensile stress-strain curve of HFRC can be described using the following equation,

$$\sigma = (1-d_{\mathrm{t}})E_{\mathrm{c}}\varepsilon, \tag{6}$$

$$d_{\mathrm{t}} = \begin{cases} 1-\rho_{\mathrm{t}}[1.2-0.2x^5], & x \leqslant 1, \\ 1-\dfrac{\rho_{\mathrm{t}}}{\alpha_{\mathrm{t}}(x-1)^{1.7}+x}, & x > 1, \end{cases}$$

$$\rho_{\mathrm{c}} = \frac{f_{\mathrm{t,H}}}{E_{\mathrm{c}}\varepsilon_{\mathrm{t,H}}},\ x = \frac{\varepsilon}{\varepsilon_{\mathrm{t,H}}}, \tag{7}$$

where σ is the tensile stress (MPa), ε is the strain; E_{c} is the elastic modulus (MPa); $f_{\mathrm{t,H}}$ is the tensile strength of HFRC (MPa); $\varepsilon_{\mathrm{t,H}}$ is the strain corresponding to the tensile strength of HFRC; d is the damage evolution parameter and is mainly dependent on the degree of plasticity x that is defined as the ratio of ε to $\varepsilon_{\mathrm{t,H}}$; α_{t} is the descending shape parameter and determines the slope of the descending branch during the post-peak stage. According to the previous literature [10], E_{c} of HFRC is assumed identical to the corresponding plain concrete in this study.

For the equation-based model of HFRC, $f_{\mathrm{t,H}}$, $\varepsilon_{\mathrm{t,H}}$, and α_{t} are the three main parameters and can be determined by back-fitting the experimental data. $f_{\mathrm{t,H}}$ and $\varepsilon_{\mathrm{t,H}}$ can be easily

obtained from the peak point of each tensile stress-strain curve. α_t needs to be determined by fitting each tensile stress-strain curve by using Eqs. (6) and (7). $f_{t,H}$, $\varepsilon_{t,H}$, and α_t of HFRC are related to steel fibers and PVA fibers [9,10]. Therefore, the back-fitting of these three parameters needs to consider the influences of steel fibers and PVA fibers on the tensile behavior of HFRC. In this study, the polynomial function is proposed, as a first approximation, to back fit the relationship between $f_{t,H}$, $\varepsilon_{t,H}$, and α_t of HFRC and the characteristics of steel fibers and PVA fibers. The fitting results are indicated in Eqs. (8)–(10).

$$f_{t,H} = f_{t,p}(1 + A),$$

$$A = 0.886\lambda_S + 0.044\lambda_P - 0.015\lambda_S\lambda_P - 0.589\lambda_S^2 - 0.008\lambda_P^2, \quad (8)$$

$$\varepsilon_{t,H} = \varepsilon_{t,p}(1 + B),$$

$$B = -0.296\lambda_S + 0.400\lambda_P + 0.999\lambda_S\lambda_P - 0.060\lambda_S^2 - 0.032\lambda_P^2, \quad (9)$$

$$\alpha_t = \frac{1}{C},$$

$$C = 9.05 - 19.99\lambda_S + 5.56\lambda_P - 3.82\lambda_S\lambda_P - 33.51\lambda_S^2 - 0.62\lambda_P^2,$$

$$\lambda_S = \frac{l_S}{d_S}V_S,\ \lambda_P = \frac{l_P}{d_P}V_P, \quad (10)$$

where $f_{t,p}$ is the tensile strength of plain concrete (MPa); $\varepsilon_{t,p}$ is the SCTS of plain concrete; λ_S is the reinforcement index of steel fibers; and λ_P is the reinforcement index of PVA fibers. l_S, d_S, and V_S are the fiber length (mm), fiber diameter (mm), and fiber volume content of steel fibers, respectively; l_P, d_P, and V_P are the fiber length (mm), fiber diameter (mm), and fiber volume content of PVA fibers, respectively.

Steel fibers and PVA fibers have a hybrid effect on the tensile behavior of HFRC [9,10,12,13], and the term $\lambda_S\lambda_P$ is introduced into Eqs. (8)–(10) to consider this hybridization of steel fibers and PVA fibers. Because $\lambda_S\lambda_P$ is the quadratic term, λ_S^2 and λ_P^2 are also listed in Eqs. (8)–(10) to keep the balance. The back-fitting results of $f_{t,H}$, $\varepsilon_{t,H}$, and α_t are presented in Fig. 7. Equations (8)–(10) can reproduce the relationship between $f_{t,H}$, $\varepsilon_{t,H}$, α_t of HFRC and the characteristics of steel fibers and PVA fibers well although the value of R^2 is not very high.

To obtain the equation-based model of HFRC, $f_{t,P}$, $\varepsilon_{t,P}$, and E_c needs to first get from the corresponding plain concrete and be acted as the reference parameters in Eqs. (8)–(10). Secondly, $f_{t,H}$, $\varepsilon_{t,H}$, and α_t could be obtained by Eqs. (8)–(10) with the fiber characteristic parameter. Then all these three parameters are fed into Eqs. (6) and (7) to plot the tensile stress-strain curve of HFRC.

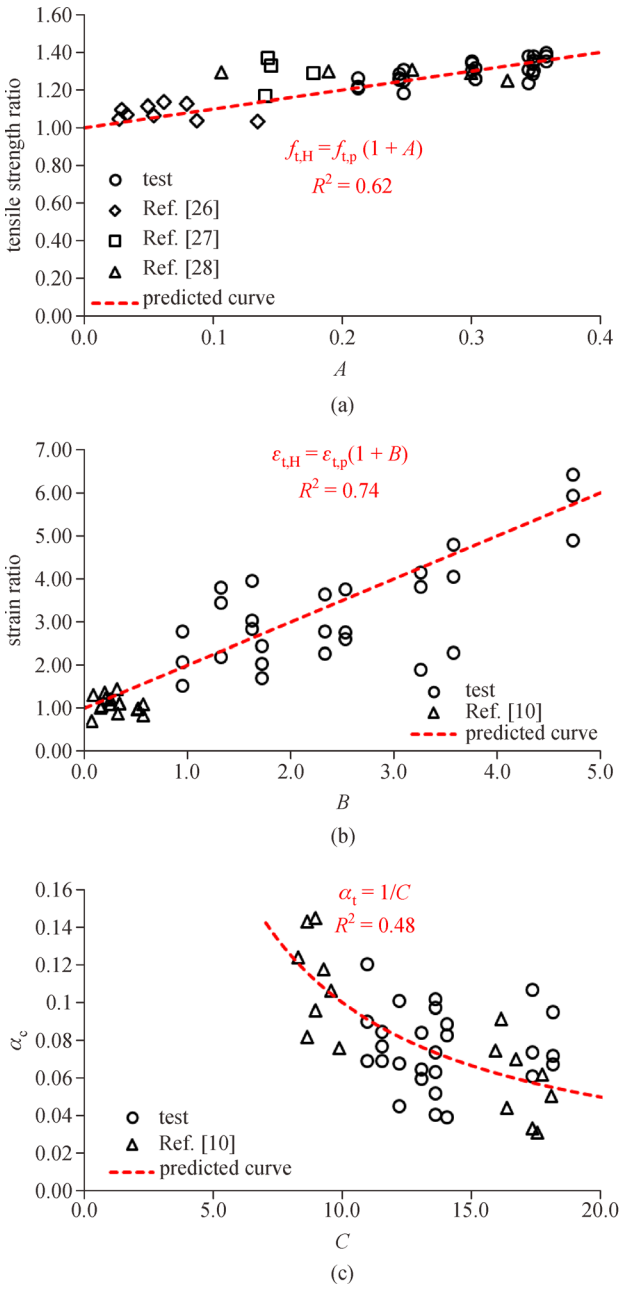

Fig. 7 Back-fitting results of key parameters in equation-based model: (a) tensile strength, $f_{t,H}$; (b) SCTS, $\varepsilon_{t,H}$; (c) descending shape parameter, α_t.

4.4 Model performance analysis

After the training of the ANN model, all input datasets are fed into the ANN model to predict the tensile stress-strain

curve, tensile strength, and SCTS of HFRC. As mentioned above, triplicate ANN models with different methods to process output features are compared in terms of predicting the tensile behavior of HFRC. The equation-based model is also used to predict the tensile stress-strain curve, tensile strength, and the corresponding strain. Then, the R^2 and *MAE* of these curves are calculated for the three different ANN models (the same architecture but different data processed methods) and the equation-based model (in Table 4), while these two indices of three methods are also included. Figure 8 shows the predicted results of the ANN model and the equation-based model as well as the experimental results of HFRC. Compared with the equation-based model, the ANN model has a better ability to reproduce the experimental results. For the ANN model, the predicted curves of the no-processed method and mid-processed method could fit better and even overlap with the experimental data, while there is a little bit gap between the predicted curves of the processed method and the test data. This is because, among the three processed methods, the no-processed method and the mid-processed method does not process the stress data and keep their original version, while the processed method normalizes the stress data. As mentioned above, the Min-Max Scaling limits the data in the range from 0 to 1 and the difference between the prediction and the test data would be amplified after inversing the Min-Max Scaling as the range expands from 0 to 4.5. For example, assuming that the prediction is 0.821 and the test data is 0.902 in the processed method of the ANN model, the gap between the prediction and the test data is 0.081 and its value is small enough to be acceptable. But after inversing the Min-Max Scaling, the prediction becomes 3.648 and the test data becomes 4 (the peak value of the ANN-Processed curve in Fig. 8(a)), and the gap increases to 0.352. This explains the phenomenon that the gap between the test data and the prediction of the processed method is larger than that of the no-processed method and the mid-processed method. The *MAE* of the processed method is larger and the R^2 of the processed method is smaller than that of the no-processed method and the mid-processed method, which can be seen in Table 4. It can also approve that normalizing the stress could enlarge the gap between the prediction and the truth.

To further evaluate the performance of the ANN model, the other two output features are also evaluated by comparing the equation-based model and the ANN model. Instead of listing the specific predictions, this study introduces the relative error [10] to evaluate the prediction of the tensile strength and SCTS, which can be seen in Fig. 9. Compared with the equation-based model, the ANN model shows a better prediction ability. The relative error of the ANN model is lower than that of the equation-based model in terms of the tensile strength and SCTS. Besides, Fig. 9 also presents the relative error of three processed methods. For the prediction of the tensile strength, all three processed methods have a very small relative error, but there is an obvious gap between these three processed methods in terms of the prediction of SCTS. The maximal relative error of the no-processed could be up to 23.8%, while the other two processed methods have a maximal value of less than 2%. This is because, in the no-processed method, the SCTS is not normalized in the data preprocessing procedure, and both the other two processed methods normalize the SCTS. The SCTS varies in a small range (from 0.00007 to 0.00068), but the minimal loss of the no-processed method is 0.00251 (Fig. 6(a)) and the minimal *MAE* of the no-processed method is 0.01698 (Fig. 6(c)). Both these two indices are much higher than that of the SCTS. Without normalization, the small range of the SCTS is difficult for the ANN model to predict when combining the large range of the tensile strength. The Min-Max Scaling would amplify the SCTS to a range from 0 to 1 and it could enable the ANN model to more easily predict the SCTS.

Table 4 *MAE*, R^2 of the ANN model and equation-based model for predicting the tensile stress-strain curve of HFRC

mix ID	*MAE*				R^2			
	ANN			equation	ANN			equation
	no-processed	mid-processed	processed		no-processed	mid-processed	processed	
$S_{0.5}P_{0.5}$	0.047	0.046	0.075	0.119	0.992	0.994	0.986	0.973
$S_{0.5}P_{1.0}$	0.045	0.050	0.094	0.199	0.996	0.995	0.977	0.929
$S_{0.5}P_{1.5}$	0.041	0.045	0.068	0.482	0.996	0.995	0.987	0.561
$S_{1.0}P_{0.5}$	0.077	0.076	0.109	0.234	0.982	0.984	0.968	0.918
$S_{1.0}P_{1.0}$	0.048	0.065	0.092	0.485	0.996	0.992	0.983	0.569
$S_{1.0}P_{1.5}$	0.068	0.059	0.143	0.692	0.989	0.992	0.955	0.350
$S_{1.5}P_{0.5}$	0.124	0.123	0.239	0.688	0.953	0.964	0.882	0.354
$S_{1.5}P_{1.0}$	0.048	0.049	0.132	0.571	0.997	0.997	0.977	0.622
$S_{1.5}P_{1.5}$	0.052	0.032	0.080	1.139	0.997	0.998	0.990	0.139

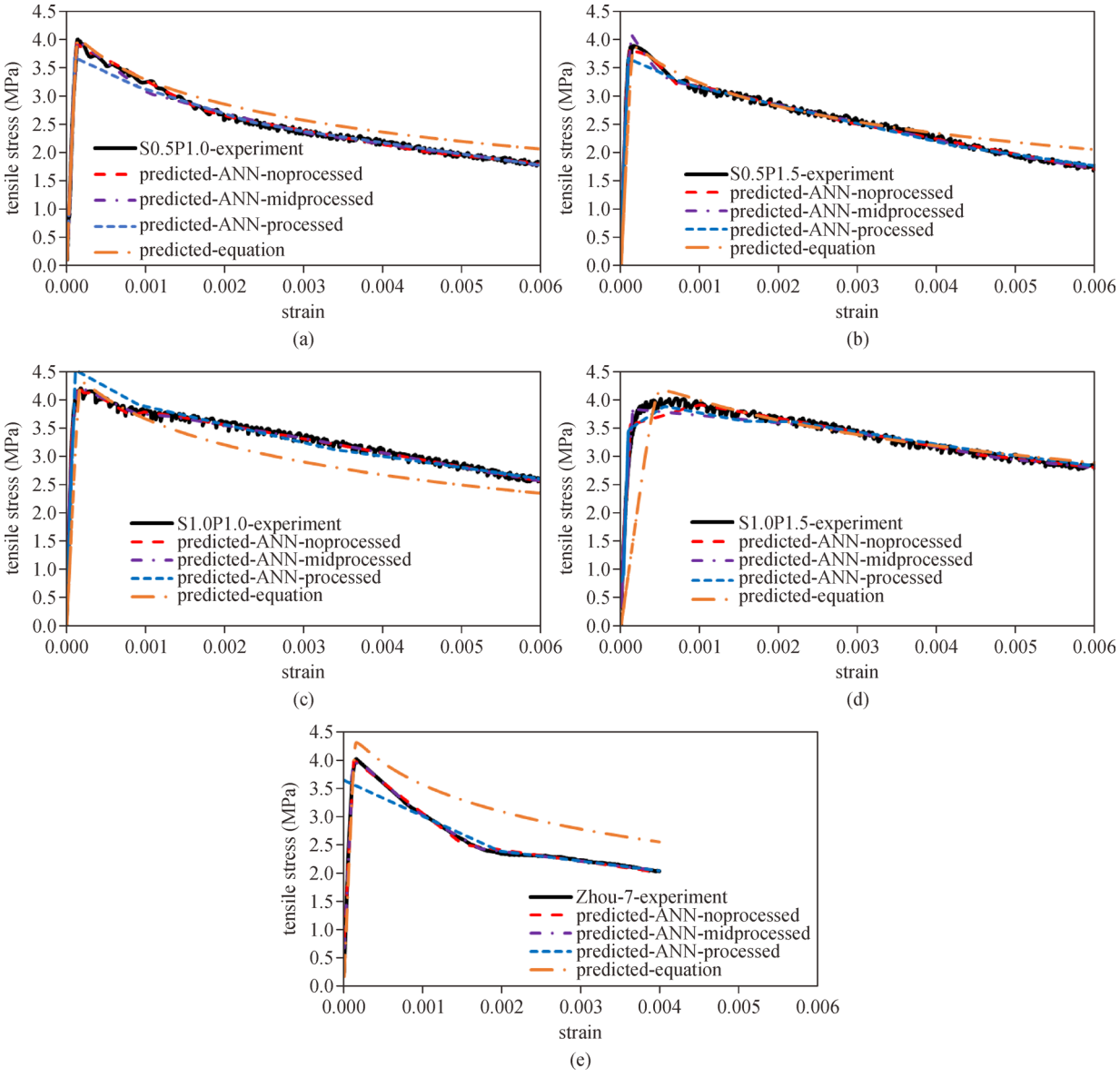

Fig. 8 Comparison of prediction results and experimental results of the tensile stress-strain curves: (a) $S_{0.5}P_{1.0}$; (b) $S_{0.5}P_{1.5}$; (c) $S_{1.0}P_{1.0}$; (d) $S_{1.0}P_{1.5}$; (e) test unit 7 reported in Ref. [10].

5 Sensitivity analysis and discussion

5.1 Sensitivity analysis

The 'PaD' method focuses on calculating the derivative of the output concerning the inputs of the ANN model [28], which can be used to highlight the contribution of the input features. These partial derivatives are called sensitivity and are defined as Eq. (11). As the ANN model in this study has one input layer, 2-hidden-layer, and one output layer, it needs the chain rule to get the final version of the sensitivity, which can be seen in Eq. (13). Once the sensitivity has been obtained for each input feature and data sample, two main indices could be calculated to analyze the results: mean sensitivity ($S_{mi,\mathrm{avg}}$), and sum squared sensitivity (SSS_{mi}). SSS_{mi}, defined in Eq. (14), is the sum squared sensitivity of the output of the mth neuron in the output layer concerning the ith input feature. Based on the sum squared sensitivity, the contribution of each input feature to each output feature could be defined as Eq. (15).

$$s_{mi}|_{X_h} = \frac{\partial o_m}{\partial x_i}(X_h), \tag{11}$$

$$o_m = \Sigma_k \omega_{mk} o_k,\ o_k = f_2\left(\sum_j \omega_{kj} o_j\right),$$

$$o_j = f_1\left(\sum_i \omega_{ji} x_i\right), \tag{12}$$

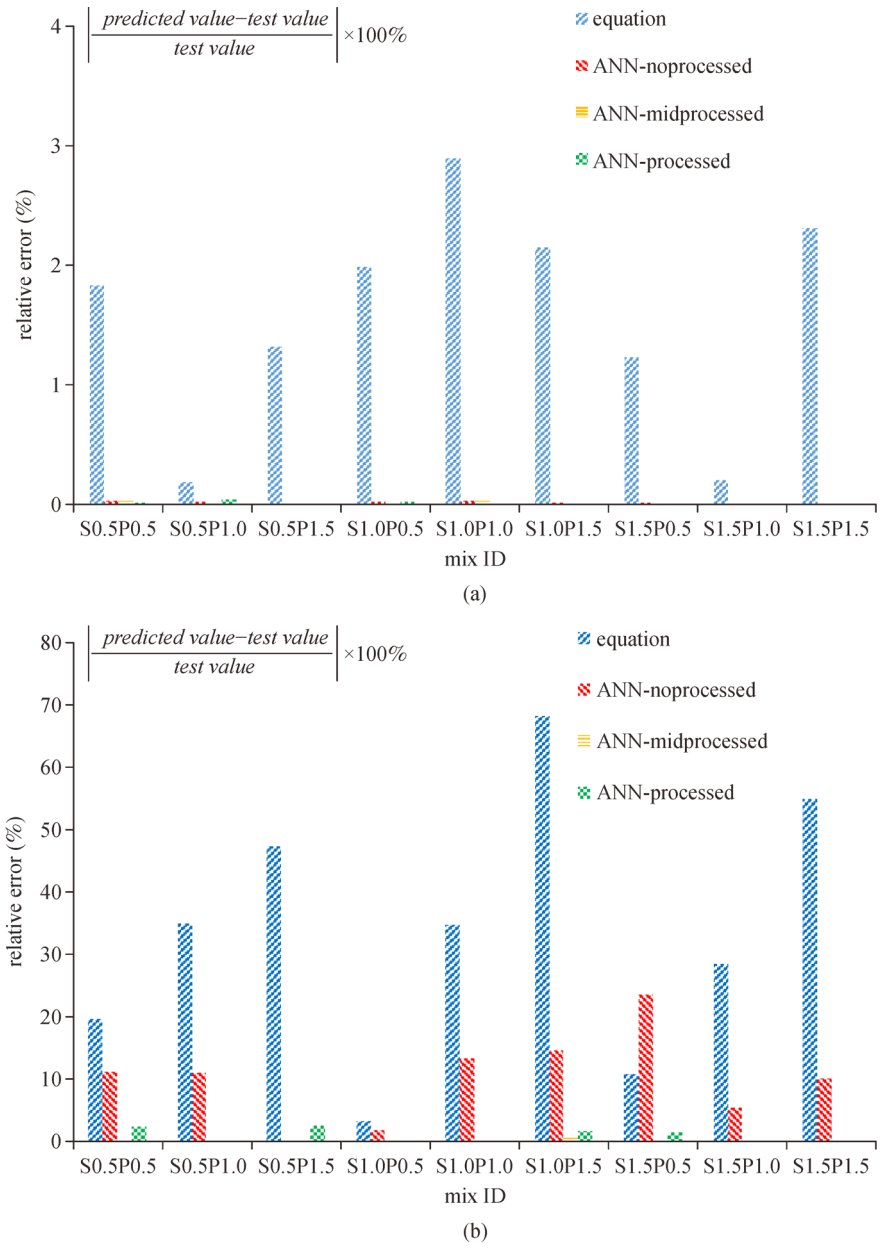

Fig. 9 The relative error of the ANN model and equation-based model in terms of (a) the tensile strength and (b) SCTS.

$$s_{mi}|_{X_h} = \frac{\partial o_m}{\partial o_k}\frac{\partial o_k}{\partial o_j}\frac{\partial o_j}{\partial x_i}(X_h), \tag{13}$$

$$SSS_{mi} = \sum_{h=1}^{N}(s_{mi}|_{X_h})^2, \tag{14}$$

$$\text{Contribution of } i\text{th input variable} = \frac{SSS_{mi}}{\sum_i SSS_{mi}}, \tag{15}$$

where N is the number of samples in the dataset; X_h is the hth sample of the dataset; $s_{mi}|_{X_h}$ is the sensitivity of the output of the mth neuron in the output layer concerning the input of the ith neuron in the input layer evaluated in X_h; X_i is the input of the ith neuron in the input layer; o_m is the output of the neuron m in the output layer; o_k is the output of the neuron k in the hidden layer II; o_j is the output of the neuron j in the hidden layer I; f_2 and f_1 are the activation functions in the hidden layer II and I; ω_{mk}, ω_{kj}, and ω_{ji} are the weight between the neuron m and the neuron k, the weight between the neuron k and the neuron j, the weight between the neuron j and the neuron i.

Figure 10 shows the contribution of each input feature to the tensile strength and SCTS for each HFRC sample. The color represents the contribution and the darker means the higher contribution. Besides, four main parts are proposed to combine similar input features to investigate the tensile behavior: steel fiber, PVA fiber, mechanical properties of plain concrete, and components of HFRC, which can be seen in Table 1. Figure 11 shows the contributions of these

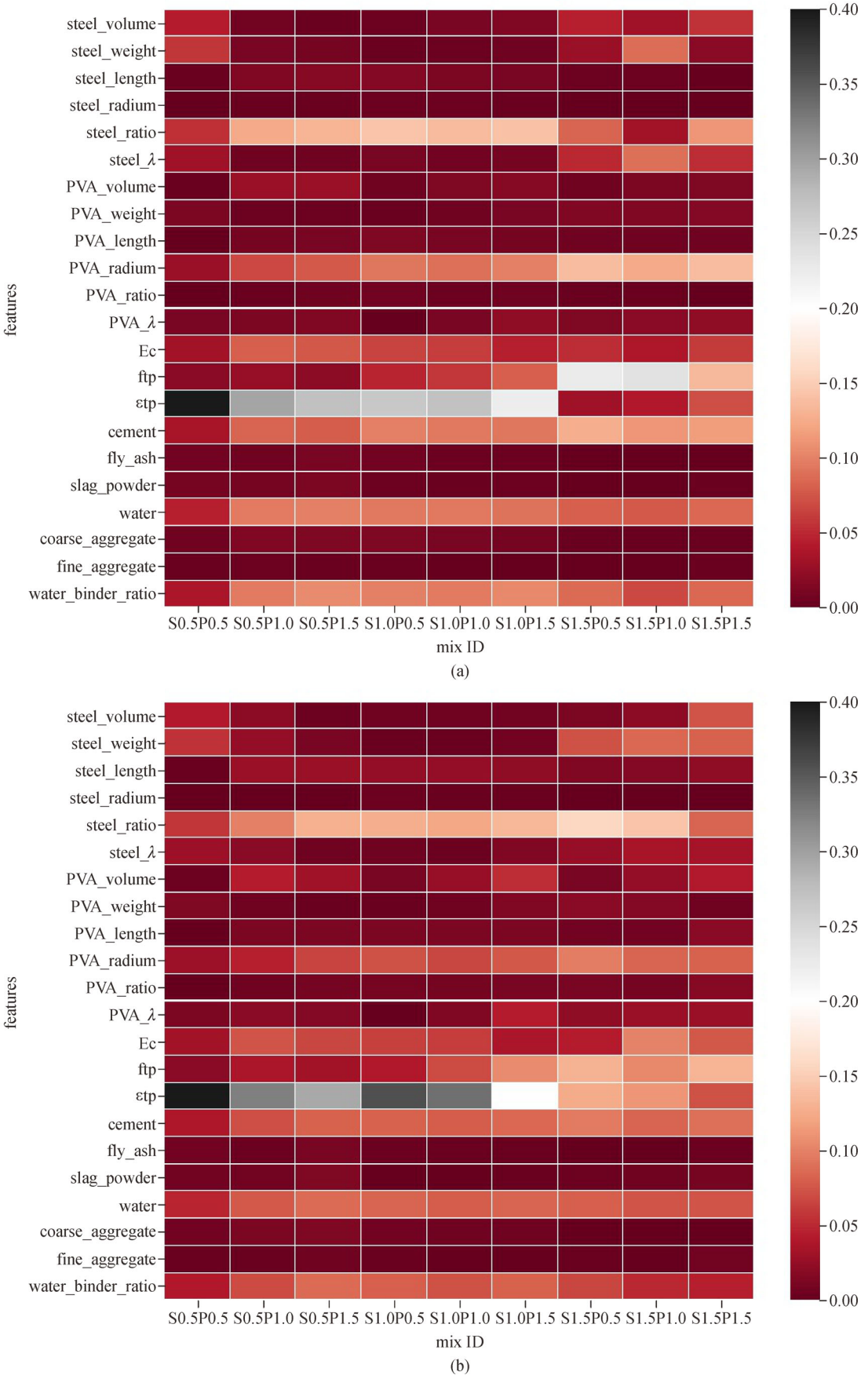

Fig. 10 Contributions of each input feature to the tensile strength and SCTS of HFRC: (a) tensile strength; (b) SCTS.

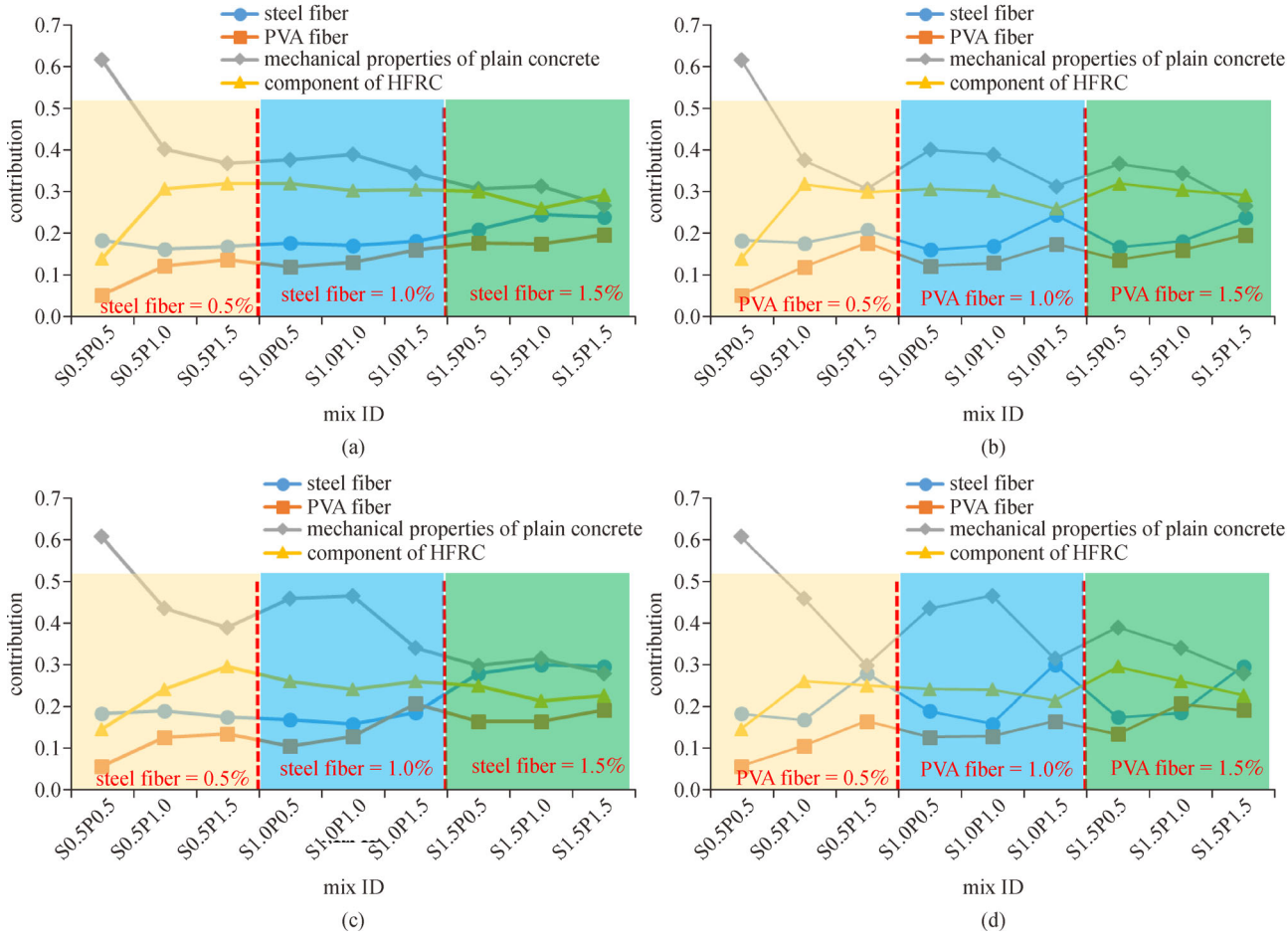

Fig. 11 Contribution of steel fibers, PVA fibers, mechanical properties of plain concrete, and components of HFRC to the tensile strength and SCTS of HFRC: (a) tensile strength as the fiber volume of steel fibers is constant; (b) tensile strength as the fiber volume of PVA fibers is constant; (c) SCTS as the fiber volume of steel fibers is constant; (d) SCTS as the fiber volume of PVA fibers is constant.

four parts to the tensile strength and SCTS for each HFRC sample and the contributions of these four parts are calculated by summarizing their input features (Table 1). According to Figs. 10 and 11, the mechanical properties of plain concrete make the main contribution to the tensile strength and SCTS among almost all HFRC samples. The contribution of steel fibers is higher than that of PVA fibers in terms of the tensile strength and SCTS. When the fiber volume of steel fibers is below 1.0%, the contributions of steel fibers to the tensile strength and SCTS remain stable and then increase as the fiber volume of steel fibers increases to 1.5%. In comparison, the contributions of PVA fibers to the tensile strength and SCTS increases gradually when adding more PVA fibers. Besides, the contributions of components of HFRC to the tensile strength and SCTS of HFRC remain stable.

5.2 Discussion

As shown in Figs. 8, 9, and Table 4, the ANN model shows a better ability to predict the tensile stress-strain curve, tensile strength, and SCTS of HFRC than the equation-based model. This is because, compared with the equation-based model, the ANN model could consider more factors (such as components of HFRC), adaptively extract more crucial input features, and present more powerfully nonlinear-fitting capacities. As the performance of the equation-based model is strongly dependent on three key parameters, $f_{t,H}$, $\varepsilon_{t,H}$, and α_t, the fitting results depend largely on the manual effect, namely, the selection of functions. In comparison, the ANN model could avoid this manual effect to a certain extent, which enables the ANN model to better describe the tensile behavior of HFRC. However, the ANN model needs a large and diverse database to improve its performance. Especially, many tensile stress-strain curves of HFRC are necessary because the ANN model is used to predict the tensile stress-strain curve of the HFRC.

Three processed methods are introduced in this study to process the output features: no-processed, mid-processed,

and processed. As mentioned above, the processed method has a worse prediction of the tensile stress than the other two methods and the no-processed method shows the worst prediction among the three methods in terms of the SCTS, while all three methods present a similar prediction of the tensile strength. Because the Min-Max Scaling method limits the data in the range from 0 to 1, it seems to have various influences on the different ranges of output features. The Min-Max Scaling is suitable for the output feature which varies in a very small range of less than 1, such as SCTS. In comparison, the output feature changing in a large range of much greater than 1, such as the stress, tends to be worsen predicted by using the Min-Max Scaling.

According to the ANN model, steel fibers tend to make a higher contribution to the tensile strength and SCTS than PVA fibers, which is similar to the experimental results that steel fibers play a more important role in the tensile behavior of HFRC [9]. Although their values are lower than that of steel fiber, the contributions of PVA fibers to the tensile strength and SCTS keep increasing whatever the fiber volume of steel fiber is.

6 Conclusions

This study builds an ANN model to describe the tensile behavior of HFRC containing fly ash and slag powder. The results of many direct tensile tests are combined with the literature data to build the database. Meanwhile, an equation-based model is also established and compared with the ANN model. Three methods to process output features are discussed and the sensitivity analysis is made to better understand the ANN model. The following conclusions can be drawn:

1) The ANN model has a better capacity of reproducing the tensile behavior of hybrid steel-PVA fiber concrete containing fly ash and slag powder than the equation-based model. The ANN model shows more powerfully non-linear-fitting abilities and could consider more factors (a total of 23 factors), including fibers' characteristics, mechanical properties of plain concrete, and concrete composition.

2) The normalization has different influences on different types of indices of the HFRC's tensile behavior. The SCTS should be normalized because it is usually very small and varies in a small range (less than one). On the contrary, the tensile stress should not be normalized as its range is often much greater than 1.

3) The ANN model can interpret the influence of different features on the tensile behavior of HFRC. Among all input features, the mechanical properties of plain concrete make the main contribution to the tensile strength and SCTS; steel fiber tends to make a higher contribution to the tensile strength and SCTS than PVA fiber. These outcomes are similar to the experimental results.

Acknowledgements The authors would like to acknowledge the National Natural Science Foundation of China (Grant Nos. 51978515, 41941018), Shanghai Sailing Program (19YF1451400), and Shanghai Municipal Science and Technology Major Project (2017SHZDZX02) for their financial support.

References

1. Gong C, Ding W, Mosalam K M, Günay S, Soga K. Comparison of the structural behavior of reinforced concrete and steel fiber reinforced concrete tunnel segmental joints. Tunnelling and Underground Space Technology, 2017, 68: 38–57
2. Stoll F, Saliba J E, Casper L E. Experimental study of CFRP-prestressed high-strength concrete bridge beams. Composite Structures, 2000, 49(2): 191–200
3. Sim J, Park C, Moon D Y. Characteristics of basalt fiber as a strengthening material for concrete structures. Composites Part B, Engineering, 2005, 36(6–7): 504–512
4. Xu L, Xu H, Chi Y, Zhang Y. Experimental study on tensile strength of steel-polypropylene hybrid fiber reinforced concrete. Advanced Science Letters, 2011, 4(3): 911–916
5. Nguyen D L, Kim D J, Ryu G S, Koh K T. Size effect on flexural behavior of ultra-high-performance hybrid fiber-reinforced concrete. Composites Part B, Engineering, 2013, 45(1): 1104–1116
6. Wu Z, Shi C, He W, Wang D. Static and dynamic compressive properties of ultra-high performance concrete (UHPC) with hybrid steel fiber reinforcements. Cement and Concrete Composites, 2017, 79: 148–157
7. Liu F, Ding W, Qiao Y. An experimental investigation on the integral waterproofing capacity of polypropylene fiber concrete with fly ash and slag powder. Construction & Building Materials, 2019, 212: 675–686
8. Mu R, Miao C, Luo X, Sun W. Interaction between loading, freeze-thaw cycles, and chloride salt attack of concrete with and without steel fiber reinforcement. Cement and Concrete Research, 2002, 32(7): 1061–1066
9. Liu F, Ding W, Qiao Y. Experimental investigation on the tensile behavior of hybrid steel-PVA fiber reinforced concrete containing fly ash and slag powder. Construction & Building Materials, 2020, 241: 118000
10. Zhou Y, Xiao Y, Gu A, Zhong G, Feng S. Orthogonal experimental investigation of steel-PVA fiber-reinforced concrete and its uniaxial constitutive model. Construction & Building Materials, 2019, 197: 615–625
11. Liu F, Ding W, Qiao Y. Experimental investigation on the flexural behavior of hybrid steel-PVA fiber reinforced concrete containing fly ash and slag powder. Construction & Building Materials, 2019, 228: 116706
12. Lawler J, Wilhelm T, Zampini D, Shah S P. Fracture processes of hybrid fiber-reinforced mortar. Materials and Structures, 2003, 36(3): 197–208
13. Lawler J S, Zampini D, Shah S P. Microfiber and macrofiber hybrid fiber-reinforced concrete. Journal of Materials in Civil Engineering, 2005, 17(5): 595–604
14. Nguyen D L, Ryu G S, Koh K T, Kim D J. Size and geometry dependent tensile behavior of ultra-high-performance fiber-reinforced concrete. Composites. Part B, Engineering, 2014, 58: 279–

292

15. Pujadas P, Blanco A, Cavalaro S, Aguado A. Plastic fibres as the only reinforcement for flat suspended slabs: Experimental investigation and numerical simulation. Construction & Building Materials, 2014, 57: 92–104
16. Hsie M, Tu C, Song P. Mechanical properties of polypropylene hybrid fiber-reinforced concrete. Materials Science and Engineering A, 2008, 494(1–2): 153–157
17. Chi Y, Xu L, Yu H. Constitutive modeling of steel-polypropylene hybrid fiber reinforced concrete using a non-associated plasticity and its numerical implementation. Composite Structures, 2014, 111: 497–509
18. Chi Y, Xu L, Zhang Y. Experimental study on hybrid fiber-reinforced concrete subjected to uniaxial compression. Journal of Materials in Civil Engineering, 2014, 26(2): 211–218
19. Açikgenç M, Ulaş M, Alyamaç K E. Using an artificial neural network to predict mix compositions of steel fiber-reinforced concrete. Arabian Journal for Science and Engineering, 2015, 40(2): 407–419
20. Mashhadban H, Kutanaei S S, Sayarinejad M A. Prediction and modeling of mechanical properties in fiber reinforced self-compacting concrete using particle swarm optimization algorithm and artificial neural network. Construction & Building Materials, 2016, 119: 277–287
21. Jiang K, Han Q, Bai Y, Du X. Data-driven ultimate conditions prediction and stress-strain model for FRP-confined concrete. Composite Structures, 2020, 242: 112094
22. Hamdia K M, Zhuang X, Rabczuk T. An efficient optimization approach for designing machine learning models based on genetic algorithm. Neural Computing & Applications, 2020 (in press)
23. Hamdia K M, Lahmer T, Nguyen-Thoi T, Rabczuk T. Predicting the fracture toughness of PNCs: A stochastic approach based on ANN and ANFIS. Computational Materials Science, 2015, 102: 304–313
24. Hamdia KM, Ghasemi H, Zhuang X, Alajlan N, Rabczuk T. Computational machine learning representation for the flexoelectricity effect in truncated pyramid structures. Computers, Materials & Continua, 2019, 59(1): 79–87
25. Guo H, Zhuang X, Rabczuk T. A deep collocation method for the bending analysis of Kirchhoff plate. Computers, Materials & Continua, 2019, 59(2): 433–456
26. Anitescu C, Atroshchenko E, Alajlan N, Rabczuk T. Artificial neural network methods for the solution of second order boundary value problems. Computers, Materials & Continua, 2019, 59(1): 345–359
27. Samaniego E, Anitescu C, Goswami S, Nguyen-Thanh V M, Guo H, Hamdia K, Zhuang X, Rabczuk T. An energy approach to the solution of partial differential equations in computational mechanics via machine learning: Concepts, implementation and applications. Computer Methods in Applied Mechanics and Engineering, 2020, 362: 112790
28. Pizarroso J, Portela J, Muñoz A. NeuralSens: Sensitivity analysis of neural networks. 2020, arXiv preprint arXiv:200211423
29. Saltelli A. Sensitivity analysis for importance assessment. Risk Analysis, 2002, 22(3): 579–590
30. Shojaeefard M H, Akbari M, Tahani M, Farhani F. Sensitivity analysis of the artificial neural network outputs in friction stir lap joining of aluminum to brass. Advances in Materials Science and Engineering, 2013, 2013: 574914
31. Stone M. Cross-validatory choice and assessment of statistical predictions. Journal of the Royal Statistical Society. Series B. Methodological, 1974, 36(2): 111–133
32. Nair V, Hinton G E. Rectified linear units improve restricted Boltzmann machines. In: Proceedings of the 27th International Conference on Machine Learning (ICML-10). Haifa, 2010, 807–814
33. Liu B. Study on Durability and Mechanical Properties of Hybrid Fiber Reinforced Concrete. Thesis for the Master's Degree. Jinzhou: Liaoning University of Technology, 2019
34. Yang K H. Tests on concrete reinforced with hybrid or monolithic steel and polyvinyl alcohol fibers. ACI Materials Journal, 2011, 108(6): 664–672
35. Hai R, Liu J, Zhang M, Zhang L. Performance of hybrid steel-polyvinyl alcohol fiber reinforced ultra high performance concrete. Concrete (China), 2016, 319: 95–97
36. Pedregosa F, Varoquaux G, Gramfort A, Michel V, Thirion B, Grisel O, Blondel M, Prettenhofer P, Weiss R, Dubourg V, Vanderplas J, Passos A, Cournapeau D, Brucher M, Perrot M, Duchesnay E. Scikit-learn: Machine learning in Python. The Journal of Machine Learning Research, 2011, 12: 2825–2830
37. Paszke A, Gross S, Massa F, Lerer A, Bradbury J, Chanan G, Killeen T, Lin Z, Gimelshein N, Antiga L, Desmaison A, Köpf A, Yang E, DeVito Z, Raison M, Tejani A, Chilamkurthy S, Steiner B, Fang L, Bai J, Chintala S. PyTorch: An imperative style, high-performance deep learning library. In: Advances in Neural Information Processing Systems. 2019, 8026–8037
38. Marian Tietz T J F, Daniel N, Benjamin B. Skorch: A Scikit-Learn Compatible Neural Network Library that Wraps PyTorch. 2017
39. Kingma D P, Ba J. Adam: A method for stochastic optimization. 2014, arXiv preprint arXiv:14126980
40. Cortes C, Vapnik V. Support-vector networks. Machine Learning, 1995, 20(3): 273–297
41. Breiman L. Random forests. Machine Learning, 2001, 45(1): 5–32
42. Rasmussen C E. Gaussian Processes in Machine Learning. Springer: Summer School on Machine Learning, 2003, 63–71
43. Chinese Standard. Code for Design of Concrete Structures (GB 50010–2010). Beijing: China Building Industry Press, 2010